High visible light sensitive MoS_2 ultrathin nanosheets for photoelectrochemical biosensing

Siyuan Wu, Hao Huang, Mengxiang Shang, Cuicui Du, Yue Wu, Wenbo Song

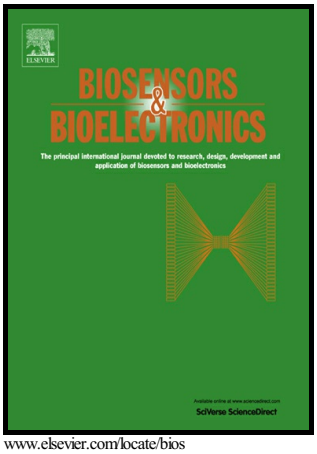

www.elsevier.com/locate/bios

PII: S0956-5663(16)31053-3
DOI: http://dx.doi.org/10.1016/j.bios.2016.10.037
Reference: BIOS9259

To appear in: *Biosensors and Bioelectronic*

Received date: 7 August 2016
Revised date: 1 October 2016
Accepted date: 18 October 2016

Cite this article as: Siyuan Wu, Hao Huang, Mengxiang Shang, Cuicui Du, Yue Wu and Wenbo Song, High visible light sensitive MoS_2 ultrathin nanosheets for photoelectrochemical biosensing, *Biosensors and Bioelectronic* http://dx.doi.org/10.1016/j.bios.2016.10.037

High visible light sensitive MoS_2 ultrathin nanosheets for photoelectrochemical biosensing

Siyuan Wu, Hao Huang, Mengxiang Shang, Cuicui Du, Yue Wu, Wenbo Song*

College of Chemistry, Jilin University, Changchun 130012, P.R. China

Corresponding author: Email: wbsong@jlu.edu.cn

Tel：+86 18626659501

Abstract

For the purpose of effectively utilizing the visible light, photoelectrochemical (PEC) detection represents a unique detection signal and different energy form of the excitation source. In this work, ultrathin MoS_2 nanosheets with narrow band gap were successfully fabricated by a facile C_3N_4 sacrificial template assisted thermolytical approach. Upon immobilizing glucose oxidase, excellent photocatalytic activity towards glucose is achieved in neutral buffer solution. As a novel visible light sensitive photocatalytic material, ultrathin MoS_2 nanosheets present a detection limit of ~0.61 nM, which is much lower than those with the similar configurations reported previously. Based on the excellent anti-interference property, the feasibility of applying the proposed sensor to determine glucose in human serum is further demonstrated. This work provides new insight into the fabrication of promising visible light sensitive two-dimensional layered transition-metal chalcogenides nanostructures for construction of photoelectrochemical biosensors.

Keywords

ultrathin MoS_2 nanosheets; visible light sensitive; photoelectrochemical biosensor; glucose

1. Introduction

As a source of energy for the living cells and metabolic intermediate, glucose is of great importance in clinical and food analysis and plays a critical role in the improvement of life quality and the public health (Shan et al. 2009; Wang 2008; Xu et al. 2007). Update, numerous detection approaches including surface plasmon resonance (Al-Ogaidi et al. 2014), fluorescence (Chang et al. 2009), electrochemistry (Shan et al. 2009) and colorimetry (Gao et al. 2007) etc. have been developed in the past several decades, and most of which are based on the enzymatic activity of new nanomaterials or nanostructures within the sensors for the purpose of fast, reliable, sensitive and low-cost glucose determination. Among these strategies, amperometric methods based on enzymatic glucose oxidation have received substantial attention, and glucose oxidase (GOD) is often used to catalyze the oxidation of glucose due to high selectivity, fast response and low cost (Su et al. 2014). However, the GOD modified bare electrodes are hardly to achieve catalytic activity and stability, while the immobilization of GOD on the sensor surface provides high reactivity and selectivity for glucose recognition (Mu et al. 2007; Riklin et al. 1995).

Photoelectrochemical (PEC) sensing is a newly appeared yet dynamically developing approach for chemical and biomolecular analysis in recent years due to its inexpensive and simple photoelectric devices (Tang et al. 2014; Yue et al. 2013). Like other well established analytical techniques such as electrochemical bioanalysis, the

PEC technique maintains the advantages of traditional electrochemical methods and offers some additional merits that could not be realized on the conventional platform. In a typical PEC cell, electrons and holes are photogenerated by sunlight and subsequently into the cathode and anode due to the separation of the excitation source (light) and the detection signal (photocurrent) (Huo et al. 2015). Because of this total separation and the different energy form of the excitation source and detection signal, PEC sensing normally exhibits improved sensitivity as well as low background.

Recently, the utilization of nanostructured materials in PEC sensing has received considerable attention. However, the prevalent photocatalytic material such as TiO_2 is far from satisfactory because of the predominant absorption in the UV region as well as the rapid recombination of the electron–hole pairs, which limits its PEC biosensing application (Devadoss et al. 2014a; Devadoss et al. 2015). To improve electrocatalytic and photophysical activity, several other nanomaterials such as semiconductor quantum dots (Pardo-Yissar et al. 2003), metal nanoparticles (Da et al. 2014) and some carbon based materials (Foo et al. 2016) have also been involved in PEC biosensors. To simplify the sensor configuration as well as the fabrication procedures, there is a demand to develop high efficiently visible light sensitive PEC materials.

Very recently, two-dimensional (2D) layered transition-metal chalcogenides (TMDs) has gained extensive attention in PEC area (Hou et al. 2013; Yin et al. 2014), since the 2D layered structure is expected beneficial to shorten the charge transport time and distance to show more efficient charge separation and transfer. As one of the most well-known TMDs, molybdenum disulphide (MoS_2) is particularly attractive

due to its narrow band gap (1.2 eV−1.9eV) (Kim et al. 2015; Wang et al. 2012) and the ability to be exfoliated into atomically thin 2D sheets that possesses large specific surface area and relatively high mobility. Compare with traditional nanomaterials such as TiO_2, which are limited by the wide band gap and can only absorb UV light that will damage the biomolecules, MoS_2 nanosheets is a novel visible light sensitive nanomaterial that maintains excellent photocatalytic activity. Because of the unique electronic and optical properties, MoS_2 nanosheets have been successfully used in the fields of water splitting (Yin et al. 2014), fast and more efficient electronic devices etc. However, the direct utilization of MoS_2 nanosheets as a visible light-sensitive material for constructing photoelectrochemical biosensors is rarely reported.

In this work, a novel MoS_2 nanosheets-based PEC biosensor design for sensitive glucose detection was demonstrates for the first time. Herein, a 3D porous network formed by ultrathin MoS_2 nanosheets with high PEC performance was achieved via a facile thermolytical approach with the aid of C_3N_4 sacrificial template (Huang et al. 2015). The microstructure and morphology of the as-prepared nanostructure were studied in detail by using some physical characterization techniques. The 3D porous framework of ultrathin MoS_2 nanosheets reveals a large surface area and a uniform porous distribution, which is conducive to the enzyme adsorption and may lead to high reactivity and selectivity for glucose recognition upon immobilizing glucose oxidase on its surface. Additionally, the porous feature may shorten the electronic diffuse distance between the ITO substrate and the redox centers to promote the electron transfer ability.

2. Experimental section

2.1 Materials and reagents

Indium tin oxide (ITO) glass was purchased from Wuhan Ge-Ao Ltd. (China). Ammonium molybdate, thiourea and melamine were purchased from Sinopharm Chemical Reagent. Glucose oxidase was obtained from Sigma-Aldrich. Other chemicals were purchased from Beijing Chemical Reagent Company.

2.2 Apparatus

The morphology and microstructure of MoS_2 nanosheets were characterized by using HITACHI SU8020 instrument scanning electron microscopy (SEM) and TecnaiF20 transmission electron microscopy (TEM). The X-ray powder diffraction (XRD) patterns were collected in reflection mode (Cu KR radiation) on shimadzu XRD-6000. X-ray Photoelectron Spectroscopy (XPS) spectra were recorded by using ESCALAB 250 spectrometer with a mono X-Ray source Al Kα excitation (1486.6 eV). Raman spectra were measured with a Horiba LabRAM HR Evolution spectrometer. UV–vis absorption spectra were measured on a GBC Cintra 10e UV–vis spectrophotometer (Australia). The thermogravimetric analysis (TGA) was carried out on a TA2050 apparatus under nitrogen with a 10° C min^{-1} heating rate. The electrochemical tests were conducted using CHI660A (CH Instruments, Inc.USA) with a typical three-electrode cell. A 500 W xenon lamp (CHFXQ500 W, Global Xenon Lamp Power) equipped with an ultra violet filter was used as the irradiation source.

2.3 Preparation of MoS_2 nanosheets

The MoS_2 nanosheets were obtained by a facile thermolytical approach with the aid of C_3N_4 sacrificial template following the previously reported method after slight modification (Huang et al. 2015). Firstly, 4.0 g of C_3N_4 sacrificial template synthesized by one-step pyrolysis of melamine in air was mixed homogeneously with 0.3 g of ammonium molybdate $(NH_4)_2MoO_4$. The mixture was subsequently heated to 300 ºC in air to obtain MoO_3/C_3N_4 intermediate, 4.0 g of which was finally mixed with 2.0 g of thiourea. Heating to 600 ºC under nitrogen and maintaining 240 min, followed by elevating to 800 ºC and maintaining 180 min, results in the final product. As a control, a similar heating process in the absence of C_3N_4 was performed to understand the contribution of C_3N_4 for the uniform and layered structure.

2.4 Fabrication of PEC sensor

The ITO glass (1 cm × 2 cm) was cleaned by acetone, ethyl alcohol and water, and then dried by nitrogen blow. To prepare the PEC sensor, the ITO slide was dip-coated with 20 μL of slurry that was obtained by mixing 1 mg of layered MoS_2, 0.5 mL dimethylformamide and 0.5 mL ultrapure water under sonication for 20min. After completely drying in air, the slide was incubated with 5 mg ml^{-1} of glucose oxidase in phosphate buffered saline (PBS, pH=7.4) overnight. The sample was then rinsed with ultrapure water and ethanol and dried with compressed N_2.

2.5 Photoelectrochemical measurements

The photoelectrochemical measurements were performed in a conventional three electrode cell, with a MoS_2 photoanode as the working electrode, using a Pt wire and a saturated calomel electrode (SCE) as the counter electrode and reference electrode,

respectively. The photocurrent measurements were conducted with a CHI660A electrochemical workstation. A 500 W Xenon lamp with a 420 nm cutoff filter was used as a light source. The incident light intensity was 100 mW cm^{-2}. The PBS (pH 7.4) was used as the electrolyte with a volume of 20mL in an electrochemical cell, and 10μL liquid with different glucose concentration was injected. The bias voltage was selected at +0.6 V (vs. SCE) to optimize the photocurrent. The time-dependent photocurrent switch was performed in PBS containing 500 nM glucose under repeated on/off visible light illumination. The long-term stability was evaluated by measuring the current over a storage period of 2 weeks at 4^{o}C. Three sensors were prepared under the same conditions for reproducibility assessment. To verify the precision of the sensor, the glucose concentration of a diluted human serum was determined and compared with that measured by the School Hospital of Jilin University.

3. Results and discussion

3.1 Characterization of ultrathin MoS_2 nanosheets

As shown in scheme 1A, the synthesis starts from pyrolysis of ammonium molybdate and a layered C_3N_4 sacrificial template under a N_2 atmosphere to guarantee a high quality of the ultrathin MoS_2 nanosheets. Initially, an essential intermediate consisting of layered g-C_3N_4 and MoO_3 nanosheets was achieved via pyrolysis, in which the layered g-C_3N_4 acts as a sacrificial template to inhibit restack of the MoS_2 sheets. Subsequently annealing sulfourea (sulfur source) and the intermediate resulted in the gradual transformation of MoO_3 nanosheets to MoS_2 while the ultrathin morphology maintained. Further annealing led to gradual decomposition of g-C_3N_4,

leaving multiform pores and generating a 3D porous structure comprised of ultrathin MoS_2 nanosheets. To evidence the morphology revolution of MoS_2 ultrathin nanosheets from g-C_3N_4 sacrificial template and the reaction precursors, the comparative SEM and TEM images of the g-C_3N_4 template, MoO_3/g-C_3N_4 intermediate (heating the mixture of g-C_3N_4 and ammonium molybdate to 300 ºC in air) were provided (Fig.S1). From the SEM, one can see that the g-C_3N_4 is characterized by densely packed layers (Fig.S1A), which might serve as an efficient template for the formation of 2D MoS_2 nanosheets. Compared with the template, the layered morphology of the MoO_3/g-C_3N_4 intermediate reserves (Fig.S1C), although the layered structure becomes somewhat disordered, potentially due to the combination of g-C_3N_4 and MoO_3. From the TEM, the g-C_3N_4 template reveals typical layered "graphene mimic" morphology (Fig.S1B). While the MoO_3/g-C_3N_4 intermediate exhibits regular MoO_3 nanoparticles on the g-C_3N_4 layers (Fig.S1D), as evidenced by the characteristic diffraction peaks of the orthorhombic MoO_3 phase (ICDD, reference number, 00-001-0706) in the XRD of MoO_3/g-C_3N_4 intermediate (Fig.S2A). The strong peak around 27.46º indicates that a large amount of layered g-C_3N_4 template exists in the reaction intermediate.

To further explore the formation process of the 3D structure composed by ultrathin MoS_2 nanosheets, thermogravimetric analysis (TGA) of the MoO_3/g-C_3N_4 intermediate together with sulfourea (Fig.S2B) was carried out. The TGA curve manifests two-step evolution processes for obtaining the 3D structure of ultrathin MoS_2 nanosheets: (1) Under 300 °C, sulfourea decomposed gradually to form a large

amount of H_2S gas, and the MoO_3 on the g-C_3N_4 layers was transformed into ultrathin MoS_2 nanosheets. (2) With the temperature increasing from 450 to 650 °C, the g-C_3N_4 template decomposed gradually and a large amount of gas was released, which leads to a 68% weight loss in TGA. The ultrathin nanosheets randomly curved to form a 3D porous structure during the process of a large amount of gas release.

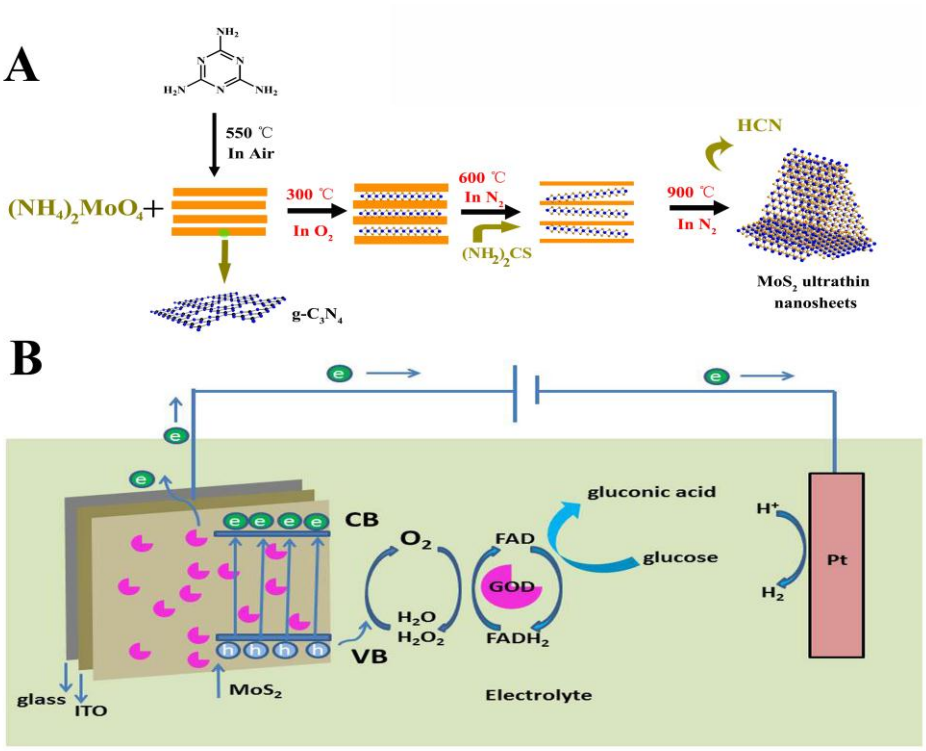

Scheme 1 (A) Proposed synthetic protocol for ultrathin MoS_2 nanosheets. 1 (B) Schematic illustration for the reaction process of the MoS_2-GOD modified ITO electrode to glucose.

Fig.1A presents the XRD pattern of 2D MoS_2 nanosheets. All diffraction peaks can be indexed to the crystalline planes of hexagonal MoS_2 (ICDD, reference number, 00-006-0097). The Raman spectrum of MoS_2 nanosheets（Fig.1B）in the informative range from 360 to 450 cm^{-1} reveals two dominant peaks at 383 and 404 cm^{-1}, which

correspond to the in-plane E^1_{2g} and out-of-plane A^1_g vibrational modes of hexagonal MoS_2. The frequency difference between E^1_{2g} and A^1_g peak is 21cm, which is far less than the 27cm of the bulk material. Previous work suggests that the frequency difference between E^1_{2g} and A^1_g Raman peak decreases stepwisely with decreasing number of the MoS_2 layers. Above result indicates that the as-prepared MoS_2 nanosheets are ultrathin.

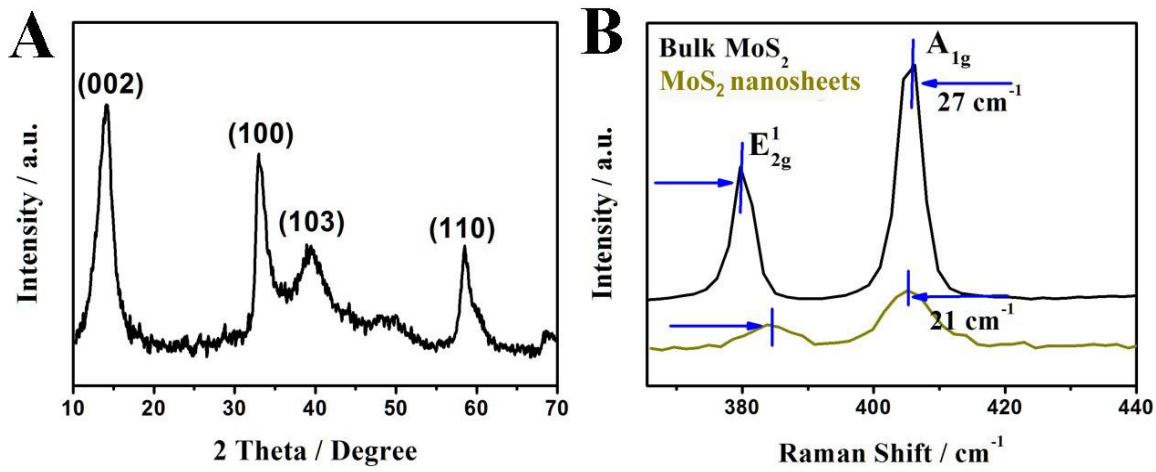

Fig.1 (A) XRD pattern of ultrathin MoS_2 nanosheets.1 (B) Comparative Raman spectra of the ultrathin MoS_2 nanosheets and bulk MoS_2.

Fig.2A shows the morphology and microstructure of the MoS_2 nanosheets characterized by scanning electron microscopy (SEM). A uniform and layered structure containing multiform pores on a larger scale can be observed obviously. Controlled experiment of heating process in the absence of C_3N_4 was also carried out to understand the contribution of C_3N_4. The XRD pattern and SEM image of the as-prepared MoS_2 without the C_3N_4 template were provided in Fig.S3. All the diffraction peaks in Fig.S3A can be indexed to the MoS_2 phase (ICDD, reference number, 00-006-0097). The peak at 14.3^o, corresponding to the (002) plane of MoS_2,

becomes broader than that of the ultrathin MoS_2 nanosheets. Heavily stacked structure was obtained for the template-free sample (Fig.S3B), indicating that the g-C_3N_4 template could effectively inhibit restacking of the MoS_2 nanosheets during thermolysis.

Fig.2B presents the typical TEM image of the sample, from which homogeneous and sheet like structure of the MoS_2 sample can be clearly seen. The TEM elemental mapping analysis confirms the homogenous distribution of Mo and S atoms with almost stoichiometric composition in the plane of MoS_2 nanosheets (Fig.2C and D). The chemical composition of the MoS_2 nanosheets is further confirmed by X-ray photoelectron spectroscopy (XPS). Fig.3A indicates that the as-prepared product contains Mo and S elements. The high-resolution XPS spectrum in Fig.3B indicated that the Mo (VI) is reduced to Mo (IV) via thermalysis: the two peaks at 229.7 and 232.8 eV are attributed to Mo 3d5/2 and Mo 3d3/2 binding energies, respectively. Fig.3C illustrates that the peaks of S 2p3/2 and S 2p1/2 binding energies located at 162.5 and 163.7 eV, respectively. The calculated atomic ratio of Mo to S in the sample approaches 1: 2.

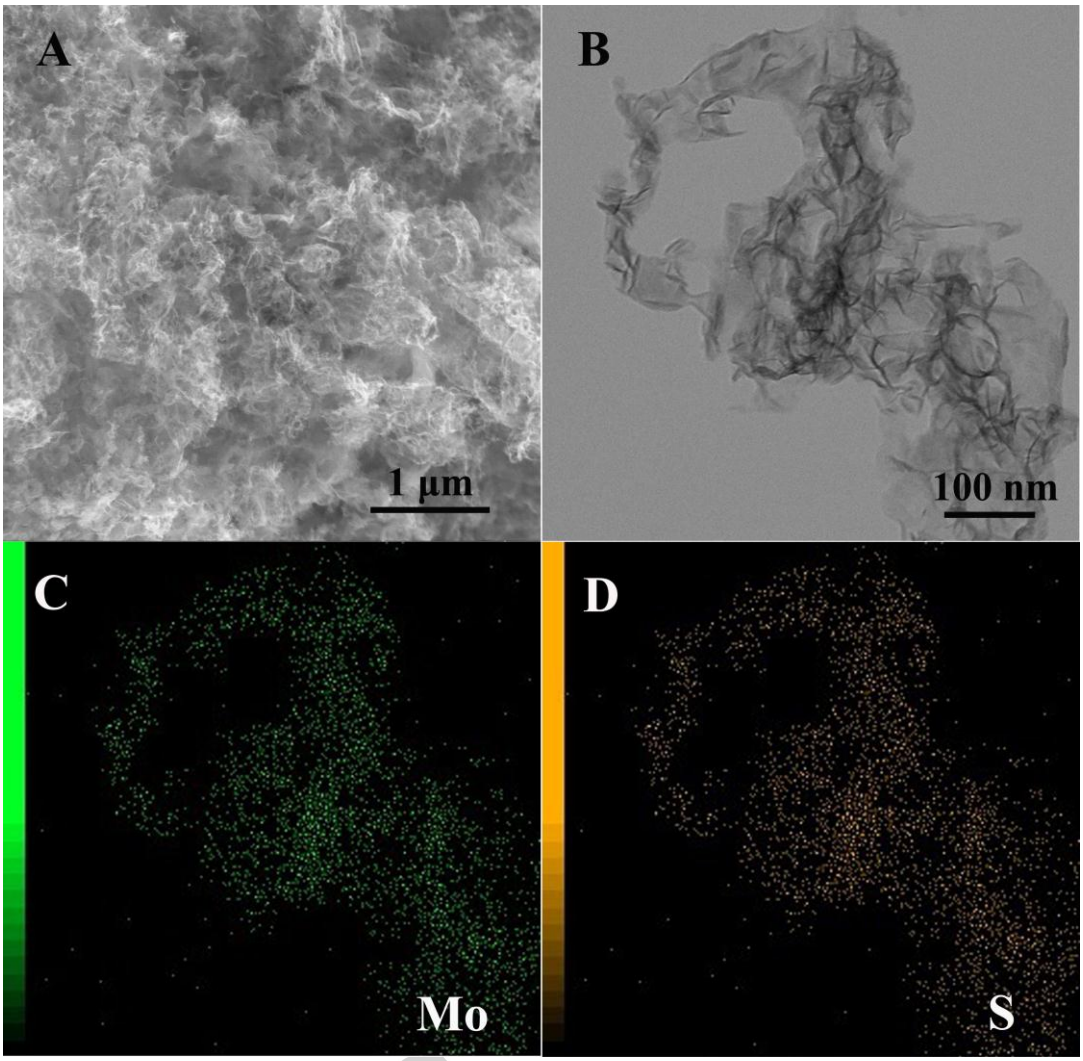

Fig.2 The images of SEM (A) and TEM (B) as well as the corresponding elemental mapping analysis (C and D) of the ultrathin MoS_2 nanosheets.

Fig.3D shows the UV–vis absorption spectrum of the MoS_2 ultrathin nanosheets. Two adsorption peaks are observed at 621nm and 680nm, and the main peak corresponds to the direct-gap of approximately 1.85 eV. While no detectable peak was observed for bulk MoS_2, since it is an indirect band gap semiconductor and the absorption peaks cannot be appeared in the UV–vis absorption region (Wang et al. 2012). Owing to the narrow band gap as well as the strong absorption in the visible

light region, the MoS_2 ultrathin nanosheets might be a promising visible light sensitive photocatalytic material for PEC sensing.

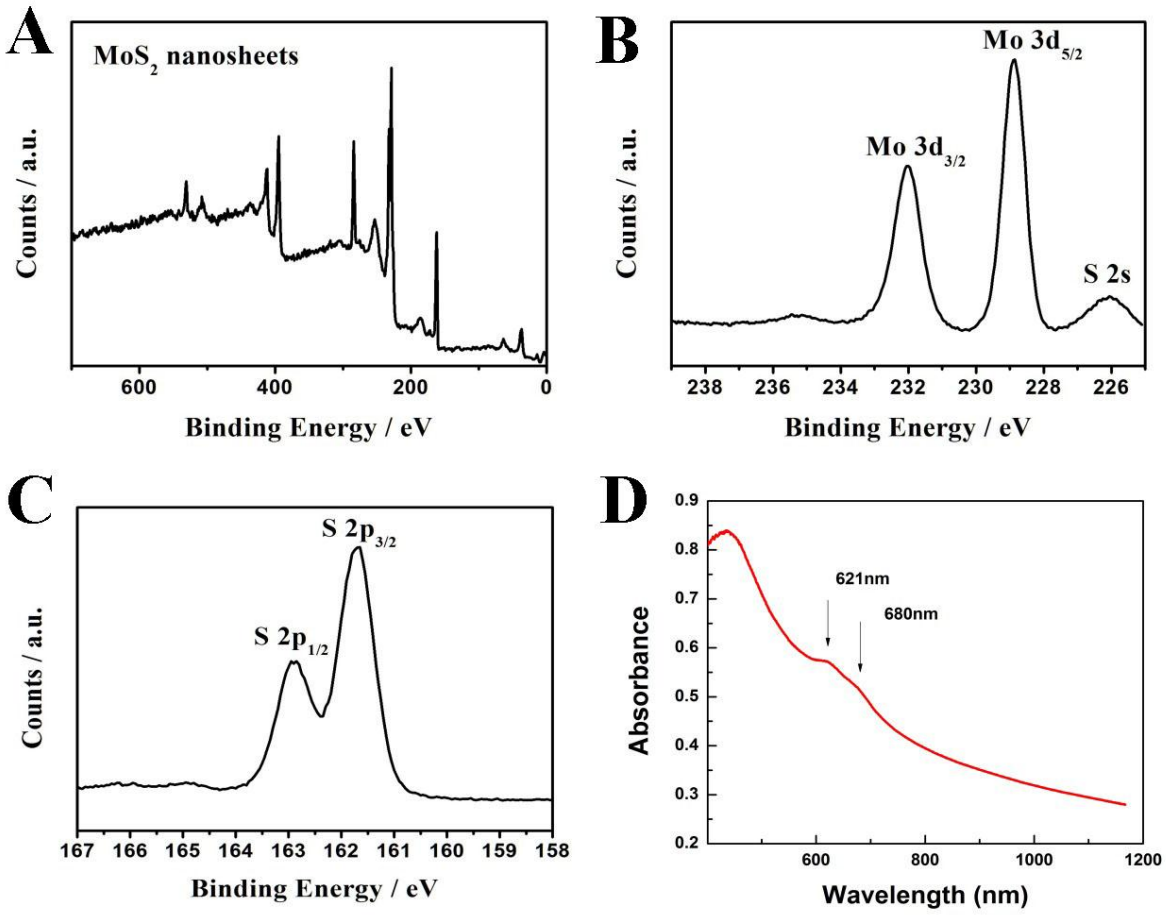

Fig.3 (A) XPS spectra of MoS_2 and high-resolution XPS spectra of Mo3d (B) and S 2p (C) of the ultrathin MoS_2 nanosheets. (D) UV–vis absorption spectra of MoS_2 nanosheets.

3.2 Principle of photoelectrochemical glucose sensing

The MoS_2 electronic band gap is around 1.85 eV, corresponding to a wavelength of around 620 nm and 680 nm, the electron-hole pairs will be generated when the wavelength of the illumination light is in the visible light region. As a proof-of-concept and based on the narrow band gap and high absorption coefficient in the visible light region, the possibility of the MoS_2 nanosheets as a novel visible light

sensitive nanomaterial for photoelectrochemical glucose detection was demonstrated for the first time. The reaction mechanism of glucose electro-oxidation catalyzed by GOD enzyme is widely accepted as follows (Clark and Lyons 1962; Sun et al. 2009; Tang et al. 2014; Xia et al. 2014): In the presence of dissolved oxygen, GOD can catalyze the electro-oxidation of glucose to produce H_2O_2. When the electrode was illuminated by the visible light, the photoexcited electron–hole pair generated in the thin film. The photo-induced hole will combine with the H_2O_2 as an electron donor to produce O_2. During these processes, O_2 serves as an efficient electron shuttling mediator between the enzymatic redox center and the sensor surface, leading to an increase of the photocurrent. Scheme 1B illustrates the reaction process of the MoS_2-GOD modified ITO electrode to glucose. The FAD redox group in GOD that is adsorbed on the surface of MoS_2 nanosheets oxidizes the glucose in solution and changes to the reduced $FADH_2$ group. When the electrode is illuminated by visible light illumination, the photo holes generated on the surface and inside of the MoS_2 films can efficiently donate holes to $FADH_2$ and regenerate the enzymatic redox center FAD, while at the same time O_2 molecules are reduced to H_2O_2. During this process, electrons are transferred immediately to the ITO substrate under an extra electrical power (Devadoss et al. 2014b; Liu et al. 2005; Tang et al. 2014).

3.3 Photoelectrochemical activity towards glucose

For the PEC sensing measurements, 0.1 M PBS buffer (pH 7.4) was used as the supporting electrolyte in a standard 3-electrode electrochemical cell, owing to the high stability of GOD at neutral pH. The area of the sensor exposed to the electrolyte

solution is defined by transparent rubber sealing and controlled at 0.50 cm^2. Since the applied potential is an important factor relevant to the photocurrent response in enzyme modified electrodes, the optimal applied potential to fetch the maximal enzyme functionality is thus determined. Fig.4A illustrates that upon addition of 100 nM glucose, the photocurrent increases with an increase in the bias potential from 0.3 to 0.6 V vs. SCE. When the applied potential is higher than +0.6 V, the photocurrent decreases gradually. Therefore, +0.6V vs. SCE is selected as the optimal potential in the subsequent study.

To evaluate the photoelectrochemical sensing possibility of the MoS_2–GOD anode, the time-dependent PEC photocurrent (i–t) measurements were carried out in 0.1 M PBS (pH 7.4) containing different glucose concentration. As shown in Fig.4B, the photocurrent is highly stable and corresponds well with the repeated on–off cycles of simulated visible light illumination under optimal conditions. When the visible light illumination is turned off, the dark current level is negligible. The photocurrent increases with the increase of the glucose concentration, suggesting a strong correlation of the redox reaction on the MoS_2-GOD surface with the glucose concentration in the solution. This result also indicates that the present glucose sensing is solely attributed to the photogenerated charge carriers.

3.4 Photoelectrochemical determination of glucose

Fig.4C shows the linear dependence of the photocurrent on MoS_2–GOD anode with the concentration of glucose injected into the PEC cell. Upon each addition of glucose, the photocurrent increases accordingly and reaches a new equilibrium within

few seconds. The lowest detectable concentration by the proposed biosensor is ~1 nM, which maintains a signal-to-noise ratio over 3 (see inset of Fig.4C). The photocurrent change with glucose concentration is summarized in the corresponding concentration-dependent calibration curve shown in Fig.4D. Inset of Fig.4D represents the linear correlation of photocurrent response with the logarithm of the glucose concentration from 8nmol/L to 5000nmol/L. The regression equation was I =1.80 +3.48 log $C_{glucose}$ (nmol/L) with the correlation coefficient of 0.992. The detection limit (LOD, S/N = 3) was estimated to be 0.61 nmol/L, which is much lower than those of the similar configurations. A comparison of the glucose linear range and detection limit for the proposed photoelectrochemical biosensor with the other similar configurations is shown in Table S1.

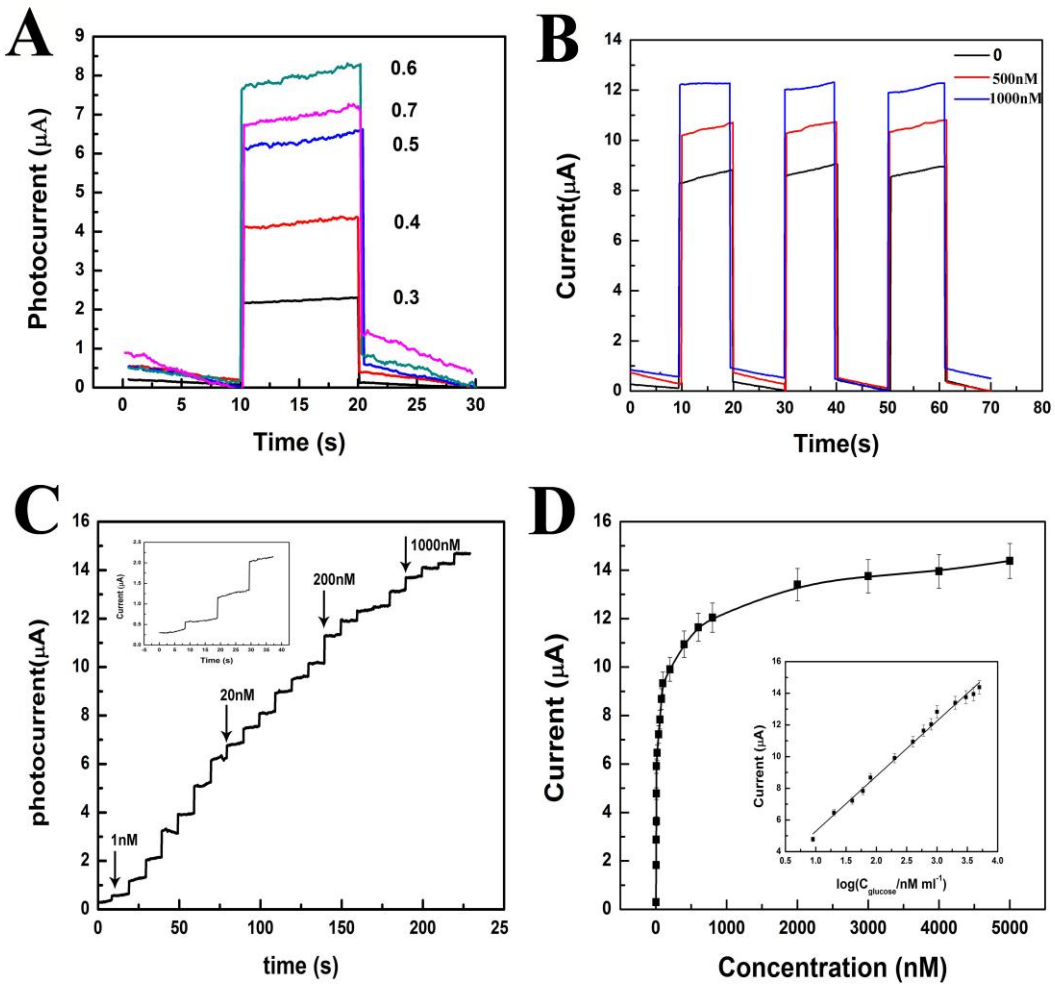

Fig.4 (A) Photocurrent generated at MoS_2 nanosheets decorated with GOD at various applied potentials. (B) Time-dependent photocurrent of a MoS_2-GOD biosensor at +0.6V vs. SCE at repeated on–off cycles of simulated visible light illumination. The glucose concentration is 0, 500, 1000 nM, respectively. (C) Photocurrent versus time for the MoS_2-GOD biosensor with successive addition of glucose under visible light illumination. Inset: photocurrent with a low glucose concentration of 1 nM. (D) Summary of the sensing signal versus glucose concentration. Inset: calibration curve for the detection of glucose with the concentration ranging from 8nmol/L to 5000nmol/L.

3.5 Selectivity, stability and reproducibility

Furthermore, the selectivity of the MoS_2–GOD sensor was proven by measuring the photocurrent response upon introducing different interferences. For instance, the introduction of 5μM of glucose analogues such as fructose, dopamine and so on does not lead to any observable photocurrent change, while much more significant signals are obtained on the addition of glucose (Fig.5A, B and C). Thus, the interference of the glucose analogues was negligible, suggesting the high selectivity of the proposed MoS_2–GOD PEC sensor. To study the stability of the sensor, the time-dependent photocurrent switch of the MoS_2-GOD electrode in the presence of 500 nM glucose was monitored under repeated on/off visible light illumination (Fig.5E). One can see that the current response remained at over 98% of the initial value after nine on/off cycles, suggesting high stability of the MoS_2-GOD sensor. To evaluate the long-term stability, the MoS_2-GOD electrode was stored at 4 ^{o}C in a dry state and the current response was measured every day. 83% current response over a storage period of 2 weeks remained (Fig.5F). For reproducibility assessment, three MoS_2-GOD electrodes were prepared under the same conditions, the relative standard deviations were calculated to be approximately 7.4%.

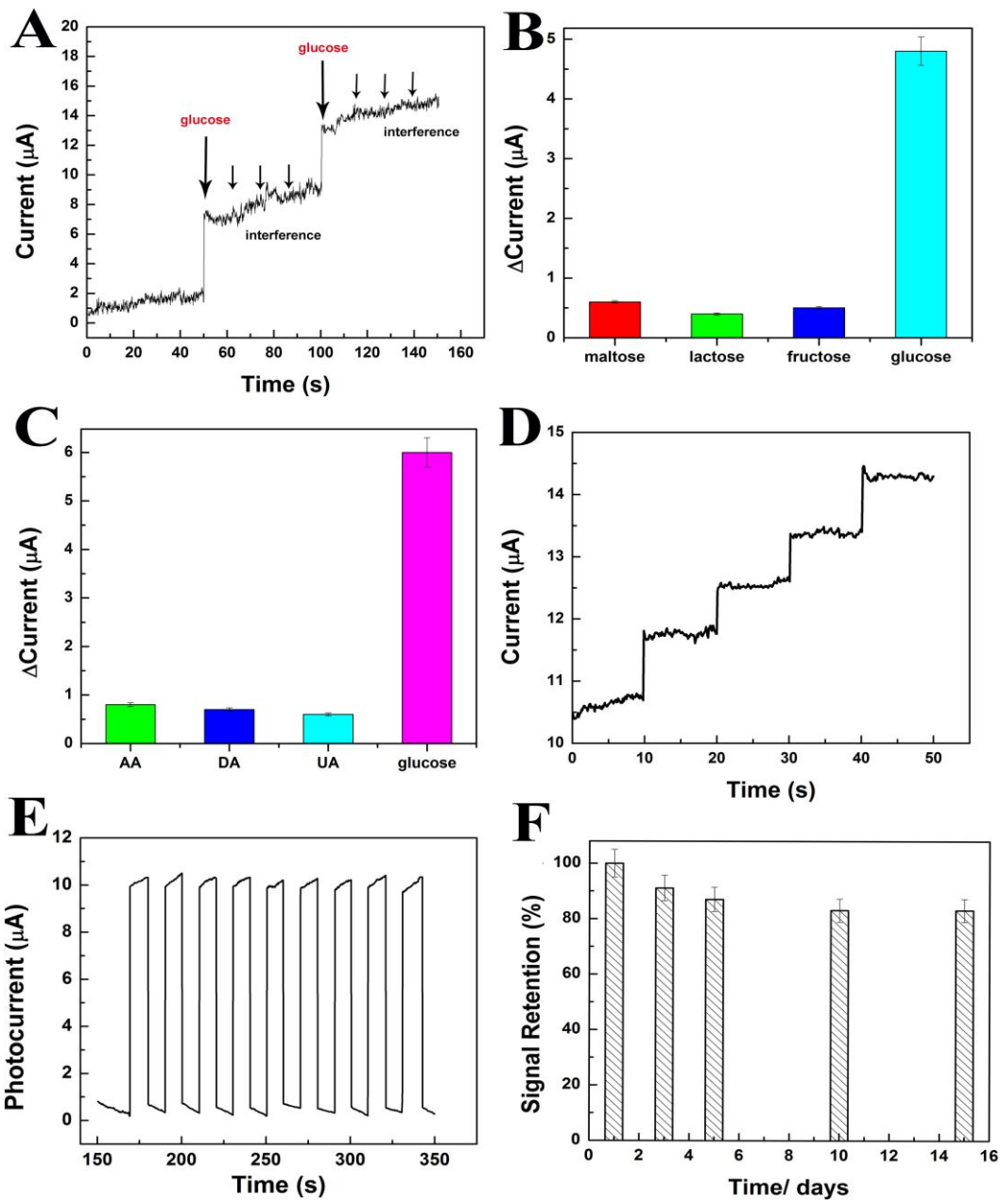

Fig.5 (A) Photocurrent versus time for the proposed biosensor with successive addition of glucose as well as other interference molecules indicated by the arrows. (B–C) Photocurrent change of the biosensor in the presence of (B) glucose analogues and (C) AA, DA, UA. The error bars represent the standard deviation for three measurements. (D) Photocurrent versus time of the biosensor for glucose detection in human serum. Each arrow indicates the addition of serum. (E) Time-dependent

photocurrent response of the MoS_2-GOD electrode in the presence of 500 nM glucose under repeated on/off visible light illumination. (F) Stability test of the MoS_2-GOD sensor over two weeks. The error bars represent the standard deviation for three measurements.

3.6. Analysis of real samples

In addition, to validate the capability of measuring glucose levels in complex body fluids for practical applications, detection of glucose in a diluted human blood serum sample was further carried out. As we all known, the blood glucose for a healthy person is 3.0–8.0 mM (Xu et al. 2007), and higher glucose values will suffer from diabetes that can damage the body and lead to multiple health problems. A clear photocurrent increase is well correlated to each addition of the serum sample, with a final diluted glucose concentration increase of ~20nM each time (Fig.5D). The glucose concentration of a diluted human serum was determined as ~4.12 mM, which is satisfactory by comparison with the value of 4.45 mM measured by the School Hospital of Jilin University. These results demonstrate that the proposed biosensor is reliable for practical determination of glucose in human serum.

Conclusion

In summary, 3D porous framework of ultrathin MoS_2 nanosheets was successfully fabricated in this work. Based on the narrow bandgap and efficient visible light sensitivity, the MoS_2 nanosheets was used as a proof-of-concept to construct high performance photoelectrochemical glucose biosensor with eliminated damage to the immobilized enzyme and biomolecules in actual test. The PEC

measurement under visible light illumination is crucial for developing safe and easy operation devices. The capability of utilizing the proposed biosensor for determining glucose in human serum is also demonstrated, suggesting the potential of developing this method for convenient, efficient and low-cost glucose monitoring and diabetes diagnosis. Substantial opportunities for further exploring other PEC biosensors based on the well-established biological interactions are also highlightened.

Acknowledgment

The authors express gratitude for the support of the National Natural Science Foundation of China (no. 21475051).

References

Shan, C., Yang, H., Song, J., Han, D., Ivaska, A., Niu, L., 2009. Anal Chem 81(6), 2378-2382.

Wang, J., 2008. Chem Rev 108(2), 814-825.

Xu, Y., Pehrsson, P.E., Chen, L.W., Zhang, R., Zhao, W., 2007. J Phys Chem C 111(24), 8638-8643.

Al-Ogaidi, I., Gou, H., Al-kazaz, A.K.A., Aguilar, Z.P., Melconian, A.K., Zheng, P., Wu, N., 2014. Anal. Chim. Acta 811, 76-80.

Chang, Q., Zhu, L., Jiang, G., Tang, H., 2009. Anal. Bioanal. Chem. 395(7), 2377-2385.

Gao, L., Zhuang, J., Nie, L., Zhang, J., Zhang, Y., Gu, N., Wang, T., Feng, J., Yang, D., Perrett, S., Yan, X., 2007. Nat. Nanotechnol. 2(9), 577-583.

Su, S., Sun, H.F., Xu, F., Yuwen, L.H., Fan, C.H., Wang, L.H., 2014. Microchim. Acta 181(13-14), 1497-1503.

Mu, C., Zhao, Q., Xu, D., Zhuang, Q., Shao, Y., 2007. J Phys Chem B 111(6), 1491-1495.

Riklin, A., Katz, E., Willner, I., Stocker, A., Buckmann, A.F., 1995. Nature 376(6542), 672-675.

Tang, J., Wang, Y., Li, J., Da, P., Geng, J., Zheng, G., 2014. J. Mater. Chem. A 2(17), 6153-6157.

Yue, Z., Lisdat, F., Parak, W.J., Hickey, S.G., Tu, L., Sabir, N., Dorfs, D., Bigall, N.C., 2013. ACS Appl Mater Interfaces 5(8), 2800-2814.

Huo, H., Xu, Z., Zhang, T., Xu, C., 2015. J. Mater. Chem. A 3(11), 5882-5888.

Devadoss, A., Sudhagar, P., Das, S., Lee, S.Y., Terashima, C., Nakata, K., Fujishima, A., Choi, W., Kang, Y.S., Paik, U., 2014a. ACS Appl Mater Interfaces 6(7), 4864-4871.

Devadoss, A., Sudhagar, P., Terashima, C., Nakata, K., Fujishima, A., 2015. J. Photochem. Photobiol., C 24, 43-63.

Pardo-Yissar, V., Katz, E., Wasserman, J., Willner, I., 2003. J Am Chem Soc 125(3), 622-623.

Da, P., Li, W., Lin, X., Wang, Y., Tang, J., Zheng, G., 2014. Anal. Chem. 86(13), 6633-6639.

Foo, C.Y., Lim, H.N., Pandikumar, A., Huang, N.M., Ng, Y.H., 2016. J. Hazard. Mater. 304, 400-408.

Hou, Y., Wen, Z., Cui, S., Guo, X., Chen, J., 2013. Adv Mater 25(43), 6291-6297.

Yin, Z., Chen, B., Bosman, M., Cao, X., Chen, J., Zheng, B., Zhang, H., 2014. Small 10(17), 3537-3543.

Kim, C., Nguyen, T.P., Le, Q.V., Jeon, J.M., Jang, H.W., Kim, S.Y., 2015. Adv. Funct. Mater. 25(28), 4512-4519.

Wang, Q.H., Kalantar-Zadeh, K., Kis, A., Coleman, J.N., Strano, M.S., 2012. Nat Nanotechnol 7(11), 699-712.

Huang, H., Feng, X., Du, C., Song, W., 2015. Chem Commun (Camb) 51(37), 7903-7906.

Clark, L.C., Jr., Lyons, C., 1962. Ann. N. Y. Acad. Sci. 102, 29-45

Sun, J.J., Zhu, Y.H., Yang, X.L., Li, C.Z., 2009. Particuology 7(5), 347-352.

Xia, L., Song, J., Xu, R., Liu, D., Dong, B., Xu, L., Song, H., 2014. Biosens Bioelectron 59, 350-357.

Devadoss, A., Sudhagar, P., Ravidhas, C., Hishinuma, R., Terashima, C., Nakata, K., Kondo, T., Shitanda, I., Yuasa, M., Fujishima, A., 2014b. Phys. Chem. Chem. Phys. 16(39), 21237-21242.

Liu, Y., Wang, M., Zhao, F., Xu, Z., Dong, S., 2005. Biosens. Bioelectron. 21(6), 984-988.

Highlight

1. Ultrathin MoS_2 nanosheets with narrow band gap were thermolytically achieved.
2. The MoS_2 is used as a high visible light sensitive material for PEC sensing.
3. The detection limit for glucose is much lower than other similar configurations.
4. The feasibility of determining glucose in human serum is demonstrated.